GeroScience (2017) 39:465–473
DOI 10.1007/s11357-017-9980-z

METHODS

Demonstration of impaired neurovascular coupling responses in TG2576 mouse model of Alzheimer's disease using functional laser speckle contrast imaging

Stefano Tarantini · Gabor A. Fulop · Tamas Kiss · Eszter Farkas · Dániel Zölei-Szénási · Veronica Galvan · Peter Toth · Anna Csiszar · Zoltan Ungvari · Andriy Yabluchanskiy

Received: 17 May 2017 / Accepted: 23 May 2017 / Published online: 3 June 2017

Abstract Increasing evidence from epidemiological, clinical, and experimental studies indicates that cerebromicrovascular dysfunction and microcirculatory damage play critical roles in the pathogenesis of many types of dementia in the elderly, including both vascular cognitive impairment (VCI) and Alzheimer's disease. Vascular contributions to cognitive impairment and dementia (VCID) include impairment of neurovascular coupling responses/functional hyperemia ("neurovascular uncoupling"). Due to the growing interest in understanding and pharmacologically targeting pathophysiological mechanisms of VCID, there is an increasing need for sensitive, easy-to-establish methods to assess neurovascular coupling responses. Laser speckle contrast imaging (LSCI) is a technique that allows rapid and minimally invasive visualization of changes in regional cerebromicrovascular blood perfusion. This type of imaging technique combines high resolution and speed to provide great spatiotemporal accuracy to measure moment-to-moment changes in cerebral blood flow induced by neuronal activation. Here, we provide detailed protocols for the successful measurement in neurovascular coupling responses in anesthetized mice equipped with a thinned-skull cranial window using LSCI. This method can be used to evaluate the effects of anti-aging or anti-AD treatments on cerebromicrovascular health.

Keywords Neurovascular coupling · Functional hyperemia · Laser speckle contrast imaging · Laser speckle contrast analysis · LASCA · Laser speckle imaging · LSI

S. Tarantini · G. A. Fulop · T. Kiss · P. Toth · A. Csiszar · Z. Ungvari · A. Yabluchanskiy (✉)
Reynolds Oklahoma Center on Aging, University of Oklahoma Health Sciences Center, 975 NE 10th Street, Oklahoma, OK 73104, USA
e-mail: andriy-yabluchanskiy@ouhsc.edu
S. Tarantini · G. A. Fulop · T. Kiss · P. Toth · A. Csiszar · Z. Ungvari · A. Yabluchanskiy
Translational Geroscience Laboratory, Department of Geriatric Medicine, University of Oklahoma Health Sciences Center, Oklahoma, OK, USA

T. Kiss · E. Farkas · D. Zölei-Szénási
Faculty of Medicine & Faculty of Science and Informatics, Department of Medical Physics and Informatics, University of Szeged, Szeged, Hungary

V. Galvan
Department of Cellular and Integrative Physiology, Barshop Institute for Longevity and Aging Studies University of Texas Health Science Center at San Antonio, San Antonio, TX, USA

P. Toth
Department of Neurosurgery, University of Pecs, Pecs, Hungary

Neurovascular uncoupling in aging and Alzheimer's disease

It is well recognized that the brain consumes more energy than any other human organ. Over 20% of the body's total energy requirements are spent to fuel the brain, which in turn only accounts for 2% of the total body mass. Moment-to-moment regulation of cerebral blood flow (CBF) is crucial since inadequate supply of glucose and oxygen to an active region of the brain

would cause cell dysfunction or injury within a very short time frame. In healthy subject during times of increased neural activity, a homeostatic mechanism termed neurovascular coupling (functional hyperemia) matches the localized demand for glucose and oxygen with increased blood supply to ensure normal brain function. Neurovascular coupling is a feed-forward mechanism which requires the coordinated cellular interaction between neurons, astrocytes, pericytes, vascular endothelial and smooth muscle cells (Petzold and Murthy 2011; Stobart et al. 2013; Wells et al. 2015; Chen et al. 2014; Tarantini et al. 2016). A large body of evidence derived from both clinical and experimental studies demonstrate that aging significantly impairs neurovascular coupling responses, which likely contribute to cognitive decline in the elderly (Balbi et al. 2015; Fabiani et al. 2013; Sorond et al. 2013; Tong et al. 2012; Toth et al. 2014; Zaletel et al. 2005; Park et al. 2007). There is also growing evidence for microvascular pathophysiological alterations having a causal role in the development of cognitive decline associated with Alzheimer's disease (AD) (Tarantini et al. 2016; Snyder et al. 2015).

An early role of vascular dysregulation in the progression of AD was underscored by recent studies of late onset AD using brain images and plasma biomarkers from the Alzheimer's Disease Imaging Initiative (ADNI) (Iturria-Medina et al. 2016). Vascular dysregulation in AD includes deficiencies in cerebrovascular reactivity, CBF, and neurovascular coupling responses (Girouard and Iadecola 2006; Gorelick et al. 2011; Hock et al. 1997; Rombouts et al. 2000). Neurovascular coupling dysfunction of AD has been replicated in experimental studies showing that in mouse models of AD, neurovascular coupling is also significantly impaired (Rancillac et al. 2012; Shin et al. 2007; Royea et al. 2017), at least in part, due to enhanced oxidative stress (Nicolakakis et al. 2008; Park et al. 2008; Park et al. 2005) arising from mitochondrial dysfunction and inflammation (Lacoste et al. 2013; Ongali et al. 2014). Importantly, recent evidence suggests that pharmacological interventions that rescue functional hyperemia result in improved cognitive function in mice with AD pathologies (Tong et al. 2012; Nicolakakis et al. 2008). Due to the increased realization that understanding of the mechanisms underlying neurovascular dysfunction is critical for developing novel therapeutic interventions to prevent or treat AD, there is an increasing need in many laboratories to adapt methodologies to investigate neurovascular coupling responses in mouse models of aging and AD (Lacoste et al. 2013; Ongali et al. 2014; Papadopoulos et al. 2016; Hamel et al. 2016; Nicolakakis and Hamel 2011; Papadopoulos et al. 2014). In this paper, published as part of the "Methods for Geroscience" series in the "Translational Geroscience" initiative of the journal (Callisaya et al. 2017; Kane et al. 2017; Kim et al. 2017; Liu et al. 2017; Meschiari et al. 2017; Perrott et al. 2017; Shobin et al. 2017; Ashpole et al. 2017; Bennis et al. 2017; Deepa et al. 2017; Grimmig et al. 2017; Hancock et al. 2017; Konopka et al. 2017; Podlutsky et al. 2017; Sierra and Kohanski 2017; Tenk et al. 2017; Ungvari et al. 2017a; Ungvari et al. 2017b; Urfer et al. 2017a; Urfer et al. 2017b), we present an easy-to-adapt protocol for assessment of neurovascular coupling responses in mice in both geroscience and AD research. As in these studies, experimental animals usually undergo behavioral testing prior to terminal experimentation; we aimed to provide a protocol that is relatively fast allowing investigators to process larger cohorts of animals. In our experience, assessment of neurovascular coupling responses in 10–15 animals per week is realistic using this protocol.

Laser speckle contrast imaging (LSCI) for assessment of neurovascular coupling responses

The accurate measurement of changes in local CBF in response to neuronal activation is essential for the assessment of the efficacy of physiological neurovascular coupling or its age- or disease-related dysfunction in experimental models. The traditional, real-time monitoring of local CBF in the cerebral cortex relies on laser Doppler flowmetry (i.e., the measurement of velocity with the aid of the frequency shift caused by the Doppler effect), which is a valid approach with excellent temporal resolution, but provides no information as to the spatial variation of flow. Still, spatial resolution is desired when a small microvascular bed responding to the activity of a distinct neuron population needs to be identified and monitored (e.g., within the barrel cortex of the mouse) (Ayata et al. 2004), or when irregular flow patterns are to be visualized in experimental models of cerebral ischemia (Bere et al. 2014). Laser Doppler flowmetry can be applied in a scanning mode to obtain two-dimensional relative flow maps (Lauritzen and Fabricius 1995), with the limitation that the mechanical

scan may not provide high enough resolution (Briers 2001; Tew et al. 2011).

As an alternative to Laser Doppler flowmetry, LSCI was first introduced for the mapping of microvascular perfusion in various tissues including the skin and the retina (Briers 2001; Ruth 1990; Tamaki et al. 1994), and was later adapted and found highly suitable to create flow maps of the superficial layers of cerebral cortex (Dunn et al. 2001). LSCI flow maps are computed using fluctuating intensity of the random interference effect known as speckle; still, LSCI and laser Doppler flowmetry both derive flow information on the basis of the same physical phenomenon and yield comparable results (Briers 2001; Tew et al. 2011). With regard to the cerebral cortex, comprehensive evaluation of LSCI against laser Doppler flowmetry has demonstrated that the two approaches deliver correlating flow data and are equally valid and powerful, with LSCI having the advantage of a good spatial resolution (Ayata et al. 2004). In particular, laser Doppler flowmetry and LSCI were found similarly suitable for the characterization of CBF changes in response to whisker stimulation, CO_2 challenge, or after middle cerebral artery occlusion in rodents (Ayata et al. 2004).

A distinct additional benefit of using LSCI is that it can be effectively combined with other imaging modalities, allowing the exact spatial and temporal correlation of optical signals. For instance, relative changes in cerebral blood volume and hemoglobin saturation can be achieved by recording intrinsic optical signals at specified wave lengths (i.e., green or red, respectively) simultaneous with CBF variations visualized by LSCI (Bere et al. 2014; Farkas et al. 2010). In addition, spectroscopic measurements using multiple wavelengths—rather than a single light source of a specific, narrow range—can yield quantitative data on hemoglobin saturation parallel with relative changes in CBF assessed by LSCI (Dunn et al. 2003). Finally, LSCI has been very successfully integrated into multi-modal imaging systems, which visualize membrane potential changes in the cerebral cortex (i.e., the intensity of the optical signal emitted by a voltage-sensitive fluorescent dye increases with decreasing transmembrane potential) (Farkas et al. 2010; Obrenovitch et al. 2009), or image variations of pH in the nervous tissue (i.e., fluorescence intensity of a pH-sensitive dye increases with deepening acidosis) (Menyhart et al. 2017). These approaches are highly pertinent and very powerful, because the exact spatial and temporal match of individual modalities offers the opportunity to draw specific conclusions about their coupling patterns (i.e., neuronal activation, metabolic status, and CBF).

Imaging apparatus

Many laboratories build their own setups for LSCI using a CCD camera with optics and custom-written image acquisition software. The protocol below was specifically optimized for experiments in geroscience and AD research for laboratories, whose primary expertise is not in cerebrovascular physiology, but who want to quickly adopt LSCI-based methods to evaluate cerebromicrovascular health and/or assess potential therapeutic interventions. The experiments shown in Fig. 1A were conducted using the commercially available high-resolution PeriCam PSI laser speckle imager (Perimed, Järfälla, Sweden) in 11-month old C57BL/6 and TG2576 mice overexpressing human APP. This device has high magnification optics, which resolves details of 20 μm/pixel in areas up to 20 × 27 mm with a fixed working distance of 10 cm. Individual data points of CBF changes in response to whisker stimulation are represented in Fig. 1B.

Experimental procedures

1) Experiments using laboratory animals must be performed in accordance with institutional and federal guidelines. The procedures described here have been approved by the Animal Care and Use Committees of the participating institutions.
2) The surgeries described in the protocol are terminal. The methods are optimized for quick processing of larger cohorts of animals. This protocol can be completed within 3 h.
3) Mouse anesthesia: The following methods of anesthesia are appropriate for assessment of neurovascular coupling measurements in rodents: (1) isoflurane (Masamoto et al. 2007), (2) ketamine (85 mg/kg, i.m.) and xylazine (3 mg/kg, i.m.) (Tong et al. 2012), and (3) alpha chloralose (Norup Nielsen and Lauritzen 2001; Hillman et al. 2007). For isoflurane use, induce anesthesia with 4% isoflurane in oxygen mix in an induction chamber using a surgical isoflurane vaporizer (Harvard Apparatus). Monitor the surgical depth by observing

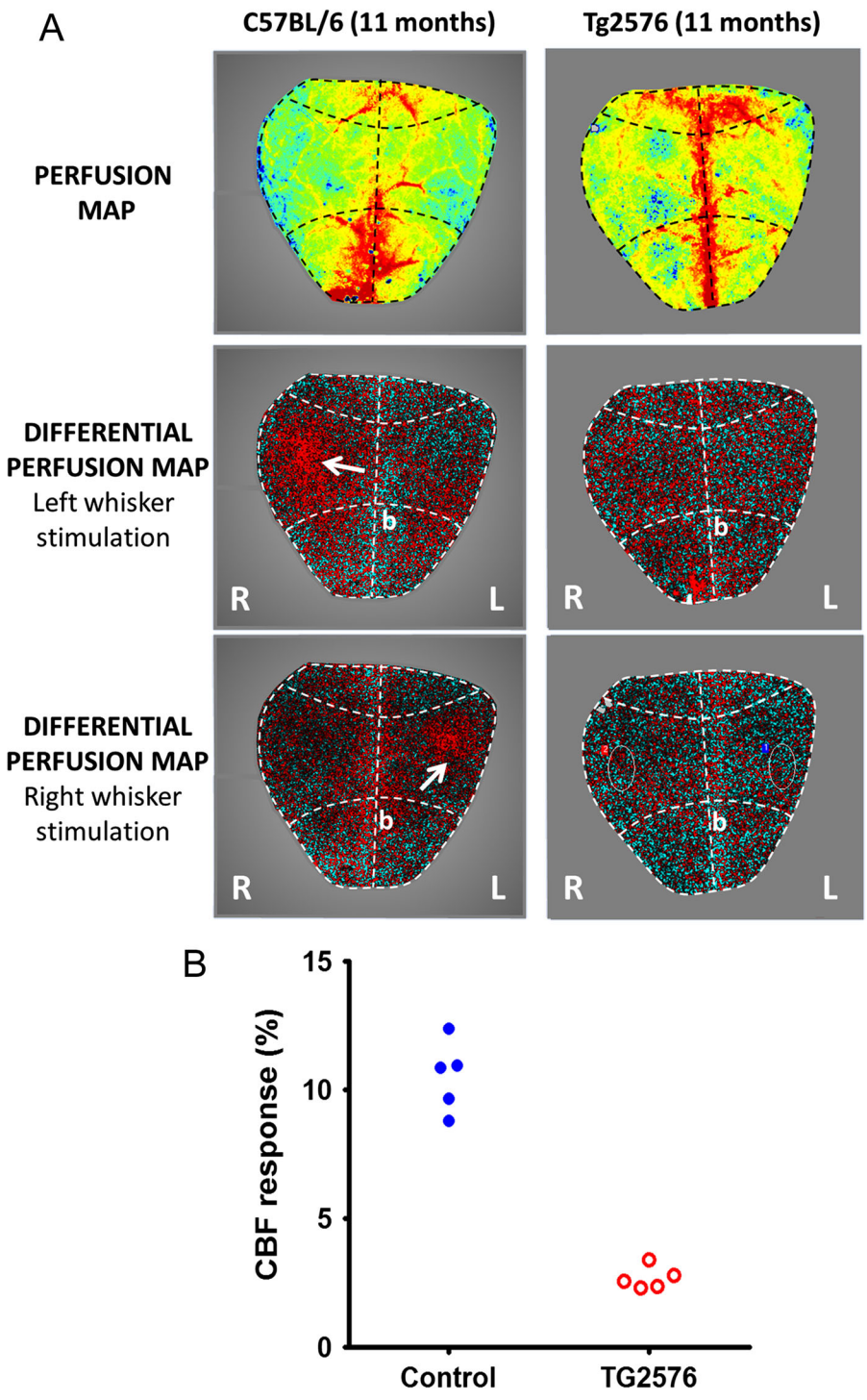

Fig. 1 **a** Representative neurovascular coupling responses between C57BL/6 and TG2576 mouse overexpressing human APP. Representative images of blood perfusion maps (*upper panel*) obtained using laser speckle contrast imaging in age-matched wild-type control (*left*) and in the mice overexpressing human amyloid precursor protein (*right*). The differential perfusion maps in the *middle* and *bottom panels* show regional increases in cerebral blood flow (*white arrows*), specifically in contralateral somatosensory whisker barrel cortex during mechanical whisker stimulation. Anatomically, the whisker barrel cortex is located 1 mm rostral and 3 mm lateral from the bregma. Thinned skull preparations do not require the skull to be completely transparent (i.e., extremely thin) as laser speckle imaging can be performed through a partially thinned and smoothed skull. **b** Overexpression of human APP in TG2576 mice results in decreased neurovascular coupling responses. The figure represents individual data points of cerebral blood flow changes in response to whisker stimulation in C57BL/6 and TG2576 mice

absence of the toe pinch reflex. Mice sedated with alpha chloralose can be first induced with 4% isoflurane, and then given a 114-mg/kg i.p. injection of alpha chloralose (Low et al. 2016; White and Field 1987). Isoflurane dose should be decreased for approximately 15 min until the alpha chloralose takes effect. Alpha chloralose can be dissolved in an 80:20 mixture of 1× phosphate

buffered saline: polyethylene glycol. At 60 min, alpha chloralose-sedated mice should be given an additional half-dose bolus. Note that alpha chloralose may have unwanted effects on heart rate and pCO_2, which may confound measurements, so careful monitoring of the animals is recommended (Low et al. 2016).

4) If desired, inject 1 mg/kg of dexamethasone (s.c., in the scruff of the neck) to reduce cerebral swelling and reduce airway secretions during surgery (Winship 2014).
5) Mice are endotracheally intubated and ventilated (MousVent G500; Kent Scientific Co., Torrington, CT). For endotracheal intubation, use the 20G plastic tube from intravenous catheter without the provided metal guide (Safelet Cath, Nipro Corp.). Connect the endotracheal tube to the mouse ventilator and monitor end-tidal CO_2 to keep blood gas values within the physiological range (Tarantini et al. 2015; Toth et al. 2015). Blood gases (pO_2 and pCO_2) and pH should be measured at the beginning and at the end of the experiment
6) Apply eye ointment (Liposic ophthalmic gel, Bausch and Lomb) onto the eyes to prevent desiccation.
7) Use a homeothermic temperature controller (Kent Scientific Co., Torrington, CT) to maintain rectal temperature at 37 °C (Toth et al. 2014).
8) Cannulate the right femoral artery to continuously monitor arterial blood pressure using a pressure transducer (Living Systems Instrumentations, Burlington, VT) (Toth et al. 2014). The femoral artery catheter can be used also for systemic drug administration or, alternatively, a venous catheter can be placed in the femoral vein.
9) Shave the skin overlying the desired imaging location.
10) Place the mouse in a stereotaxic frame (Leica Microsystems, Buffalo Grove, IL).
11) Inject 0.01 ml of the local anesthetic bupivicaine (5 mg/ml in saline, s.c.) at the incision path. Make a 1-cm longitudinal incision along the midline of the skull. Pull aside the skin to expose the skull and hold in place with bulldog serrefines. Remove the periosteum with fine forceps; clean the surface

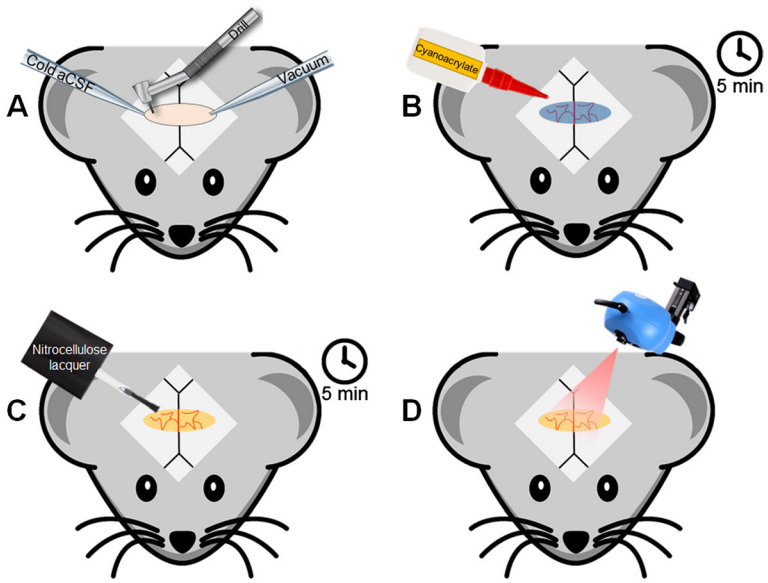

Fig. 2 Illustration of the procedures for preparation of an acute thinned-skull closed cranial window for laser speckle contrast imaging. **a** Place the mouse into stereotaxic frame. Remove the hair and perform the midline skin incision and retract the skin to expose the skull surface. Thin the skull over the brain region of interest (over the whisker barrel cortex) on both sides using a precision dental drill. Use cold artificial CSF to prevent overheating. **b** Once the skull is thinned, wipe-dry the skull surface and apply a drop of cyanoacrylate evenly over the cranial window and allow it to dry for 5 min. **c** Once cured, cover the cyanoacrylate layer with nitrocellulose lacquer and allow to dry for 5 min. **d** Position the laser speckle contrast imager 10 cm above the cranial window

of the skull with sterile gauze and cotton tip applicators until dry and clear of blood.

12) Define the borders of the planned thinned-skull cranial window using a permanent marker.
13) Use a precision dental drill for thinning the skull over the region of interest until translucent. To avoid producing excess heat and potentially damaging the brain, continually move the drill bit around region of interest, using a stochastic pattern. Regularly flush the thinned area with cold HEPES-buffered ACSF to avoid heat-induced damage to the superficial layers of the brain (Fig. 2A). Use a scalpel for the final stages of thinning. The thickness of the skull is appropriate for LSCI when pial vessels are visible. HEPES-buffered ACSF: in 500 ml of distilled H_2O, NaCl 3.94 g, KCl 0.2 g, $MgCl_2 \times 6H_2O$ 0.102 g, $CaCl_2 \times 2H_2O$ 0.132 g, NaHEPES 0.651 g; adjust the pH to 7.4.
14) Once the skull is thinned, wipe dry the surface and apply a drop of cyanoacrylate (Fig. 2B). Once cured (after 5 min), administer a thin layer of nitrocellulose lacquer to the skull to allow for even light spread on the thinned bone surface (Fig. 2C). An alternative would be to apply a layer of low-melt agarose and cover it with a coverslip.
15) After 5 more minutes of curing time, place the mouse and frame under the laser speckle contrast imager (Perimed, Järfälla, Sweden) for imaging (Fig. 2D). The laser speckle contrast imager is placed 10 cm above the thinned skull.
16) The depth of the anesthesia should be monitored throughout the experiment (tail pinch). If isoflurane anesthesia is used at this time the isoflurane is lowered to 1% maintenance dose. Higher dose of isoflurane may result in loss of autoregulation. The arterial blood pressure should be monitored and be within the physiological range throughout the experiments (90–110 mmHg).
17) Acquire a stable baseline CBF measurement.
18) To achieve the highest CBF responses, the right whiskers/whisker pad can be stimulated either mechanically of electrically. For mechanical stimulation of the whiskers, a cotton swab is used to carefully and gently brush the mouse whiskers from side to side for 30 s at ~5 Hz while recording the changes in blood flow. Alternatively, the right whisker pad can also be stimulated by a bipolar stimulating electrode placed to the ramus infraorbitalis of the trigeminal nerve and into the masticatory muscles. The stimulation protocol used to investigate neurovascular coupling consists of ten stimulation presentation trials with an intertrial interval of 70 s, each delivering a 30-s train of electrical pulses (2 Hz, 0.2 mA, intensity, and 0.3-ms pulse width) to the mystacial pad after a 10-s prestimulation baseline period.
19) Capture differential perfusion maps of the brain surface. Changes in CBF should be assessed above the left barrel cortex in ~six trials, separated by 5 min intervals. Specific neurovascular coupling responses are manifested in a well-defined region in the contralateral barrel cortex (Fig. 2). To demonstrate specificity of the responses in Fig. 2, the simultaneous measurement of blood flow changes to unilateral whisker stimulation in both hemispheres is shown. It is recommended that the side of whisker stimulation be alternated once to check the contralateral responses.
20) Average changes in CBF and express the values as percent (%) increase from the baseline value (Kazama et al. 2004). It is recommended that the experimenter be blinded to the treatment of the animals.
21) At the end of the experiments, transcardially perfuse and decapitate the animal. The brains should be immediately removed and hemisected for subsequent biochemical and histological analyses (e.g., measurement of AD-specific brain biomarkers).

Acknowledgement This work was supported by grants from the American Heart Association (to ST, MNVA, AC, and ZU), National Center for Complementary and Alternative Medicine (R01-AT006526 to ZU), National Institute on Aging (R01-AG047879 to AC; R01-AG038747), NIA-supported Geroscience Training Program in Oklahoma (T32AG052363), NIA-supported Oklahoma Nathan Shock Center (3P30AG050911-02S1), National Institute of Neurological Disorders and Stroke (NINDS; R01-NS056218 to AC), Oklahoma Shared Clinical and Translational Resources (to AY; NIGMS U54GM104938), Oklahoma Center for the Advancement of Science and Technology (to AC, ZU, and AY), the Reynolds Foundation (to ZU, AC, and AY), and the Presbyterian Health Foundation (to AC, ZU, and AY). We also acknowledge support from the Merit Review Award I01 BX002211-01A2 from the US Department of Veterans Affairs (to VG), William & Ella Owens Medical Research Foundation (VG), San Antonio Nathan Shock Center of Excellence in the

Biology of Aging (2 P30 AG013319-21) (VG), and the Robert L. Bailey and daughter Lisa K. Bailey Alzheimer's Fund in memory of Jo Nell Bailey (VG). This work was also supported by the National Research, Development and Innovation Office of Hungary (Grant No. K111923); the Bolyai János Research Scholarship of the Hungarian Academy of Sciences (No. BO/00327/14/5, to EF); and the EU-funded Hungarian Grant No. EFOP-3.6.1-16-2016-00008.

References

Ashpole NM, Logan S, Yabluchanskiy A, Mitschelen MC, Yan H, Farley JA, Hodges EL, Ungvari Z, Csiszar A, Chen S, Georgescu C, Hubbard GB, Ikeno Y, Sonntag WE. Igf-1 has sexually dimorphic, pleiotropic, and time-dependent effects on healthspan, pathology, and lifespan. Geroscience. 2017

Ayata C, Dunn AK, Gursoy OY, Huang Z, Boas DA, Moskowitz MA (2004) Laser speckle flowmetry for the study of cerebrovascular physiology in normal and ischemic mouse cortex. J Cereb Blood Flow Metab 24:744–755

Balbi M, Ghosh M, Longden TA, Jativa Vega M, Gesierich B, Hellal F, Lourbopoulos A, Nelson MT, Plesnila N (2015) Dysfunction of mouse cerebral arteries during early aging. J Cereb Blood Flow Metab 35:1445–1453

Bennis MT, Schneider A, Victoria B, Do A, Wiesenborn DS, Spinel L, Gesing A, Kopchick JJ, Siddiqi SA, Masternak MM (2017) The role of transplanted visceral fat from the long-lived growth hormone receptor knockout mice on insulin signaling. Geroscience 39:51–59

Bere Z, Obrenovitch TP, Kozak G, Bari F, Farkas E (2014) Imaging reveals the focal area of spreading depolarizations and a variety of hemodynamic responses in a rat microembolic stroke model. J Cereb Blood Flow Metab 34: 1695–1705

Briers JD (2001) Laser Doppler, speckle and related techniques for blood perfusion mapping and imaging. Physiol Meas 22: R35–R66

Callisaya ML, Launay CP, Srikanth VK, Verghese J, Allali G, Beauchet O. Cognitive status, fast walking speed and walking speed reserve-the gait and Alzheimer interactions tracking (gait) study. Geroscience. 2017

Chen BR, Kozberg MG, Bouchard MB, Shaik MA, Hillman EM (2014) A critical role for the vascular endothelium in functional neurovascular coupling in the brain. J Am Heart Assoc 3:e000787

Deepa SS, Bhaskaran S, Espinoza S, Brooks SV, McArdle A, Jackson MJ, Van Remmen H, Richardson A. A new mouse model of frailty: The Cu/Zn superoxide dismutase knockout mouse. Geroscience. 2017

Dunn AK, Bolay H, Moskowitz MA, Boas DA (2001) Dynamic imaging of cerebral blood flow using laser speckle. J Cereb Blood Flow Metab 21:195–201

Dunn AK, Devor A, Bolay H, Andermann ML, Moskowitz MA, Dale AM, Boas DA (2003) Simultaneous imaging of total cerebral hemoglobin concentration, oxygenation, and blood flow during functional activation. Opt Lett 28:28–30

Fabiani M, Gordon BA, Maclin EL, Pearson MA, Brumback-Peltz CR, Low KA, McAuley E, Sutton BP, Kramer AF, Gratton G. Neurovascular coupling in normal aging: A combined optical, erp and fmri study. Neuroimage. 2013

Farkas E, Bari F, Obrenovitch TP (2010) Multi-modal imaging of anoxic depolarization and hemodynamic changes induced by cardiac arrest in the rat cerebral cortex. NeuroImage 51:734–742

Girouard H, Iadecola C (2006) Neurovascular coupling in the normal brain and in hypertension, stroke, and alzheimer disease. J Appl Physiol (1985) 100:328–335

Gorelick PB, Scuteri A, Black SE, Decarli C, Greenberg SM, Iadecola C, Launer LJ, Laurent S, Lopez OL, Nyenhuis D, Petersen RC, Schneider JA, Tzourio C, Arnett DK, Bennett DA, Chui HC, Higashida RT, Lindquist R, Nilsson PM, Roman GC, Sellke FW, Seshadri S, American Heart Association Stroke Council CoE, Prevention CoCNCoCR, Intervention, Council on Cardiovascular S, Anesthesia (2011) Vascular contributions to cognitive impairment and dementia: a statement for healthcare professionals from the American Heart Association/American Stroke Association. Stroke 42:2672–2713

Grimmig B, Kim SH, Nash K, Bickford PC, Douglas SR (2017) Neuroprotective mechanisms of astaxanthin: a potential therapeutic role in preserving cognitive function in age and neurodegeneration. Geroscience 39:19–32

Hamel E, Royea J, Ongali B, Tong XK (2016) Neurovascular and cognitive failure in Alzheimer's disease: benefits of cardiovascular therapy. Cell Mol Neurobiol 36:219–232

Hancock SE, Friedrich MG, Mitchell TW, Truscott RJ, Else PL (2017) The phospholipid composition of the human entorhinal cortex remains relatively stable over 80 years of adult aging. Geroscience 39:73–82

Hillman EM, Devor A, Bouchard MB, Dunn AK, Krauss GW, Skoch J, Bacskai BJ, Dale AM, Boas DA (2007) Depth-resolved optical imaging and microscopy of vascular compartment dynamics during somatosensory stimulation. NeuroImage 35:89–104

Hock C, Villringer K, Muller-Spahn F, Wenzel R, Heekeren H, Schuh-Hofer S, Hofmann M, Minoshima S, Schwaiger M, Dirnagl U, Villringer A (1997) Decrease in parietal cerebral hemoglobin oxygenation during performance of a verbal fluency task in patients with Alzheimer's disease monitored by means of near-infrared spectroscopy (NIRS)—correlation with simultaneous rCBF-PET measurements. Brain res 755: 293–303

Iturria-Medina Y, Sotero RC, Toussaint PJ, Mateos-Perez JM, Evans AC (2016) Alzheimer's disease neuroimaging. I. Early role of vascular dysregulation on late-onset Alzheimer's disease based on multifactorial data-driven analysis. Nat Commun 7:11934

Kane AE, Gregson E, Theou O, Rockwood K, Howlett SE. The association between frailty, the metabolic syndrome, and mortality over the lifespan. Geroscience. 2017

Kazama K, Anrather J, Zhou P, Girouard H, Frys K, Milner TA, Iadecola C (2004) Angiotensin II impairs neurovascular coupling in neocortex through NADPH oxidase-derived radicals. Circ res 95:1019–1026

Kim S, Myers L, Wyckoff J, Cherry KE, Jazwinski SM (2017) The frailty index outperforms DNA methylation age and its

derivatives as an indicator of biological age. Geroscience 39: 83–92

Konopka AR, Laurin JL, Musci RV, Wolff CA, Reid JJ, Biela LM, Zhang Q, Peelor FF, 3rd, Melby CL, Hamilton KL, Miller BF. Influence of Nrf2 activators on subcellular skeletal muscle protein and DNA synthesis rates after 6 weeks of milk protein feeding in older adults. Geroscience. 2017

Lacoste B, Tong XK, Lahjouji K, Couture R, Hamel E (2013) Cognitive and cerebrovascular improvements following kinin B1 receptor blockade in Alzheimer's disease mice. J Neuroinflammation 10:57

Lauritzen M, Fabricius M (1995) Real-time laser-Doppler perfusion imaging of cortical spreading depression in rat neocortex. Neuroreport 6:1271–1273

Liu X, Bhatt T, Wang S, Yang F, Pai YC (2017) Retention of the "first-trial effect" in gait-slip among community-living older adults. Geroscience 39:93–102

Low LA, Bauer LC, Klaunberg BA (2016) Comparing the effects of isoflurane and alpha chloralose upon mouse physiology. PLoS One 11:e0154936

Masamoto K, Kim T, Fukuda M, Wang P, Kim SG (2007) Relationship between neural, vascular, and bold signals in isoflurane-anesthetized rat somatosensory cortex. Cereb Cortex 17:942–950

Menyhart A, Zolei-Szenasi D, Puskas T, Makra P, Orsolya MT, Szepes BE, Toth R, Ivankovits-Kiss O, Obrenovitch TP, Bari F, Farkas E (2017) Spreading depolarization remarkably exacerbates ischemia-induced tissue acidosis in the young and aged rat brain. Sci rep 7:1154

Meschiari CA, Ero OK, Pan H, Finkel T, Lindsey ML (2017) The impact of aging on cardiac extracellular matrix. Geroscience 39:7–18

Nicolakakis N, Hamel E (2011) Neurovascular function in Alzheimer's disease patients and experimental models. J Cereb Blood Flow Metab 31:1354–1370

Nicolakakis N, Aboulkassim T, Ongali B, Lecrux C, Fernandes P, Rosa-Neto P, Tong XK, Hamel E (2008) Complete rescue of cerebrovascular function in aged Alzheimer's disease transgenic mice by antioxidants and pioglitazone, a peroxisome proliferator-activated receptor gamma agonist. J Neurosci 28: 9287–9296

Norup Nielsen A, Lauritzen M (2001) Coupling and uncoupling of activity-dependent increases of neuronal activity and blood flow in rat somatosensory cortex. J Physiol 533:773–785

Obrenovitch TP, Chen S, Farkas E (2009) Simultaneous, live imaging of cortical spreading depression and associated cerebral blood flow changes, by combining voltage-sensitive dye and laser speckle contrast methods. NeuroImage 45:68–74

Ongali B, Nicolakakis N, Tong XK, Aboulkassim T, Papadopoulos P, Rosa-Neto P, Lecrux C, Imboden H, Hamel E (2014) Angiotensin ii type 1 receptor blocker losartan prevents and rescues cerebrovascular, neuropathological and cognitive deficits in an Alzheimer's disease model. Neurobiol dis 68:126–136

Papadopoulos P, Tong XK, Hamel E (2014) Selective benefits of simvastatin in bitransgenic appswe,ind/tgf-beta1 mice. Neurobiol Aging 35:203–212

Papadopoulos P, Tong XK, Imboden H, Hamel E. Losartan improves cerebrovascular function in a mouse model of Alzheimer's disease with combined overproduction of amyloid-beta and transforming growth factor-beta1. J Cereb Blood Flow Metab. 2016:271678X16658489

Park L, Anrather J, Zhou P, Frys K, Pitstick R, Younkin S, Carlson GA, Iadecola C (2005) NADPH-oxidase-derived reactive oxygen species mediate the cerebrovascular dysfunction induced by the amyloid beta peptide. J Neurosci 25:1769–1777

Park L, Anrather J, Girouard H, Zhou P, Iadecola C (2007) Nox2-derived reactive oxygen species mediate neurovascular dysregulation in the aging mouse brain. J Cereb Blood Flow Metab 27:1908–1918

Park L, Zhou P, Pitstick R, Capone C, Anrather J, Norris EH, Younkin L, Younkin S, Carlson G, McEwen BS, Iadecola C (2008) Nox2-derived radicals contribute to neurovascular and behavioral dysfunction in mice overexpressing the amyloid precursor protein. Proc Natl Acad Sci USA 105:1347–1352

Perrott KM, Wiley CD Desprez PY, Campisi J. Apigenin suppresses the senescence-associated secretory phenotype and paracrine effects on breast cancer cells. Geroscience. 2017

Petzold GC, Murthy VN (2011) Role of astrocytes in neurovascular coupling. Neuron 71:782–797

Podlutsky A, Valcarcel-Ares MN, Yancey K, Podlutskaya V, Nagykaldi E, Gautam T, Miller RA, Sonntag WE, Csiszar A, Ungvari Z. The GH/IGF-1 axis in a critical period early in life determines cellular DNA repair capacity by altering transcriptional regulation of DNA repair-related genes: Implications for the developmental origins of cancer. Geroscience. 2017

Rancillac A, Geoffroy H, Rossier J (2012) Impaired neurovascular coupling in the appxps1 mouse model of Alzheimer's disease. Curr Alzheimer res 9:1221–1230

Rombouts SA, Barkhof F, Veltman DJ, Machielsen WC, Witter MP, Bierlaagh MA, Lazeron RH, Valk J, Scheltens P (2000) Functional MR imaging in Alzheimer's disease during memory encoding. AJNR am J Neuroradiol 21:1869–1875

Royea J, Zhang L, Tong XK, Hamel E. Angiotensin IV receptors mediate the cognitive and cerebrovascular benefits of losartan in a mouse model of Alzheimer's disease. J Neurosci. 2017

Ruth B (1990) Blood flow determination by the laser speckle method. Int J Microcirc Clin Exp 9:21–45

Shin HK, Jones PB, Garcia-Alloza M, Borrelli L, Greenberg SM, Bacskai BJ, Frosch MP, Hyman BT, Moskowitz MA, Ayata C (2007) Age-dependent cerebrovascular dysfunction in a transgenic mouse model of cerebral amyloid angiopathy. Brain 130:2310–2319

Shobin E, Bowley MP, Estrada LI, Heyworth NC, Orczykowski ME, Eldridge SA, Calderazzo SM, Mortazavi F, Moore TL, Rosene DL. Microglia activation and phagocytosis: relationship with aging and cognitive impairment in the rhesus monkey. Geroscience. 2017

Sierra F, Kohanski R (2017) Geroscience and the trans-NIH geroscience interest group, GSIG. Geroscience 39:1–5

Snyder HM, Corriveau RA, Craft S, Faber JE, Greenberg SM, Knopman D, Lamb BT, Montine TJ, Nedergaard M, Schaffer CB, Schneider JA, Wellington C, Wilcock DM, Zipfel GJ, Zlokovic B, Bain LJ, Bosetti F, Galis ZS, Koroshetz W, Carrillo MC (2015) Vascular contributions to cognitive impairment and dementia including Alzheimer's disease. Alzheimers Dement 11:710–717

Sorond FA, Hurwitz S, Salat DH, Greve DN, Fisher ND. Neurovascular coupling, cerebral white matter integrity, and response to cocoa in older people. Neurology. 2013

Stobart JL, Lu L, Anderson HD, Mori H, Anderson CM (2013) Astrocyte-induced cortical vasodilation is mediated by D-serine and endothelial nitric oxide synthase. Proc Natl Acad Sci USA 110:3149–3154

Tamaki Y, Araie M, Kawamoto E, Eguchi S, Fujii H (1994) Noncontact, two-dimensional measurement of retinal microcirculation using laser speckle phenomenon. Invest Ophthalmol Vis Sci 35:3825–3834

Tarantini S, Hertelendy P, Tucsek Z, Valcarcel-Ares MN, Smith N, Menyhart A, Farkas E, Hodges E, Towner R, Deak F, Sonntag WE, Csiszar A, Ungvari Z, Toth P (2015) Pharmacologically-induced neurovascular uncoupling is associated with cognitive impairment in mice. J Cereb Blood Flow Metab 35:1871–1881

Tarantini S, Tran CH, Gordon GR, Ungvari Z, Csiszar A (2016) Impaired neurovascular coupling in aging and Alzheimer's disease: contribution of astrocyte dysfunction and endothelial impairment to cognitive decline. Exp Gerontol. doi:10.1016/j.exger.2016.1011.1004

Tenk J, Rostas I, Furedi N, Miko A, Solymar M, Soos S, Gaszner B, Feller D, Szekely M, Petervari E, Balasko M (2017) Age-related changes in central effects of corticotropin-releasing factor (CRF) suggest a role for this mediator in aging anorexia and cachexia. Geroscience 39:61–72

Tew GA, Klonizakis M, Crank H, Briers JD, Hodges GJ (2011) Comparison of laser speckle contrast imaging with laser Doppler for assessing microvascular function. Microvasc res 82:326–332

Tong XK, Lecrux C, Rosa-Neto P, Hamel E (2012) Age-dependent rescue by simvastatin of Alzheimer's disease cerebrovascular and memory deficits. J Neurosci 32:4705–4715

Toth P, Tarantini S, Tucsek Z, Ashpole NM, Sosnowska D, Gautam T, Ballabh P, Koller A, Sonntag WE, Csiszar A, Ungvari ZI (2014) Resveratrol treatment rescues neurovascular coupling in aged mice: role of improved cerebromicrovascular endothelial function and down-regulation of NADPH oxidase. Am J Physiol Heart Circ Physiol 306:H299–H308

Toth P, Tarantini S, Ashpole NM, Tucsek Z, Milne GL, Valcarcel-Ares NM, Menyhart A, Farkas E, Sonntag WE, Csiszar A, Ungvari Z (2015) IGF-1 deficiency impairs neurovascular coupling in mice: implications for cerebromicrovascular aging. Aging Cell 14:1034–1044

Ungvari Z, Tarantini S, Hertelendy P, Valcarcel-Ares MN, Fulop GA, Logan S, Kiss T, Farkas E, Csiszar A, Yabluchanskiy A (2017a) Cerebromicrovascular dysfunction predicts cognitive decline and gait abnormalities in a mouse model of whole brain irradiation-induced accelerated brain senescence. Geroscience 39:33–42

Ungvari Z, Tarantini S, Hertelendy P, Valcarcel-Ares MN, Fülöp GÁ, Logan S, Kiss T, Farkas E, Csiszar A, Yabluchanskiy A. Cerebromicrovascular dysfunction predicts cognitive decline and gait abnormalities in a mouse model of whole brain irradiation-induced accelerated brain senescence. GeroScience. 2017b:in press

Urfer SR, Kaeberlein TL, Mailheau S, Bergman PJ, Creevy KE, Promislow DE, Kaeberlein M (2017a) A randomized controlled trial to establish effects of short-term rapamycin treatment in 24 middle-aged companion dogs. Geroscience

Urfer SR, Kaeberlein TL, Mailheau S, Bergman PJ, Creevy KE, Promislow DE, Kaeberlein M (2017b) Asymptomatic heart valve dysfunction in healthy middle-aged companion dogs and its implications for cardiac aging. Geroscience 39:43–50

Wells JA, Christie IN, Hosford PS, Huckstepp RT, Angelova PR, Vihko P, Cork SC, Abramov AY, Teschemacher AG, Kasparov S, Lythgoe MF, Gourine AV (2015) A critical role for purinergic signalling in the mechanisms underlying generation of bold fMRI responses. J Neurosci 35:5284–5292

White WJ, Field KJ (1987) Anesthesia and surgery of laboratory animals. Vet Clin North Am Small Anim Pract 17:989–1017

Winship IR (2014) Laser speckle contrast imaging to measure changes in cerebral blood flow. Methods Mol Biol 1135:223–235

Zaletel M, Strucl M, Pretnar-Oblak J, Zvan B (2005) Age-related changes in the relationship between visual evoked potentials and visually evoked cerebral blood flow velocity response. Funct Neurol 20:115–120